WPPFC-CPR(18) 18770

S Ratynskaia et al.

Interaction of adhered beryllium proxy dust with transient and stationary plasmas

Preprint of Paper to be submitted for publication in Proceeding of 23rd International Conference on Plasma Surface Interactions in Controlled Fusion Devices (PSI-23)

This work has been carried out within the framework of the EUROfusion Consortium and has received funding from the Euratom research and training programme 2014-2018 under grant agreement No 633053. The views and opinions expressed herein do not necessarily reflect those of the European Commission.

Interaction of adhered beryllium proxy dust with transient and stationary plasmas

S. Ratynskaia,[1] P. Tolias,[1] M. De Angeli,[2] D. Ripamonti,[3] G. Riva,[3] D. Aussems,[4] and T. W. Morgan[4]

[1] *Space and Plasma Physics - KTH Royal Institute of Technology, Teknikringen 31, 10044 Stockholm, Sweden*
[2] *Istituto di Fisica del Plasma - Consiglio Nazionale delle Ricerche, via Cozzi 53, 20125 Milan, Italy*
[3] *Institute of Condensed Matter Chemistry and Energy Technologies - Consiglio Nazionale delle Ricerche, via Cozzi 53, 20125 Milan, Italy*
[4] *DIFFER - Dutch Institute For Fundamental Energy Research, De Zaale 20, 5612 AJ Eindhoven, The Netherlands*

Abstract

Tungsten (W) substrates with adhered beryllium (Be) proxy dust - copper, chromium, aluminium - have been exposed in the Magnum-PSI linear device. Their interaction with transient and stationary plasmas has been systematically studied under varying heat fluxes and magnetic field topologies. The dust remobilization activities, macro-morphological changes and chemical modifications induced by the plasma incidence are documented. Aluminium is identified to be the most suitable surrogate material due to the similar binary phase diagram and nearly identical evaporation rates. The results suggest that Be dust cannot survive on hot W surfaces but it can trigger mixed Be/W effects prior to its plasma removal.

1. Introduction

The tungsten and beryllium dust inventory limits in ITER have been established on the basis of safety considerations during potential accident scenarios [1, 2, 3]. These safety limits concern the total mobilizable amount of dust inside the vacuum vessel (imposed by the environmental release of hazardous respirable particulates) and the quantity of dust residing on hot surfaces (imposed by the explosion risk due to enhanced chemical reactivity with steam at elevated temperatures) [1]. In order to ensure that the latter - more stringent - limit is respected during ITER discharges, the survivability of W and Be dust residing on W divertor surfaces after the incidence of intense stationary and transient heat fluxes needs to be investigated.

The interaction of μm-size W dust adhered to bulk W surfaces with transient plasma heat loads has been systematically studied in tokamaks (DIII-D, ASDEX-Upgrade, COMPASS) and linear devices (Pilot-PSI) [4, 5, 6, 7, 8]. The experimental observations that have been supported by theoretical arguments or heat transfer simulations can be summarized as follows: **(i)** Adhered W dust and especially clusters melt under much lower heat loads than bulk W owing to the small contact area and imperfect thermal contact. **(ii)** W clusters can be transformed into large spherical W dust through the wetting induced coagulation mechanism, which arises from the competition between the fast resolidification rates and slower liquid spreading dynamics. **(iii)** W dust remobilization is inhibited by contact strengthening due to macroscopic material flow and microscopic atomic diffusion. Altogether, it has been concluded that, within the experimentally accessible parameter range, adhered W dust can survive repetitive ELM impacts and then becomes hardly mobilizable. This does not necessarily imply a violation of safety limits, since W dust generation is currently predicted to be restricted [9].

On the other hand, the Be first wall is expected to be the primary source of dust in ITER [9]. Recent simulations of the redistribution of Be droplets generated by mitigated major disruptions and vertical displacement events carried out with the MIGRAINe dust dynamics code have predicted that at least 70% of the resolidified dust mass will ultimately reside near the divertor strike point [10]. Thus, the hot surface safety limit could be exceeded provided that adhered Be dust also exhibits strong survivability. Unfortunately, the elucidated behavior of the W-on-W system under transients cannot be adopted for the Be-on-W system, where: **(i)** the much lower melting point implies a longer dust resolidification timescale that could favor complete droplet wetting or droplet ejection, **(ii)** the much higher vapor pressure and smaller atomic mass implies a stronger vaporization rate, **(iii)** the different materials imply that chemical effects could come into play. It is evident that dedicated experiments need to be performed.

The interaction of μm-size Be dust adhered to bulk W surfaces with transient plasma heat fluxes has been previously studied via surrogate materials; copper, chromium in ASDEX-Upgrade [8] and aluminium in DIII-D [11]. These exposures concerned modest heat loads and involved rather limited statistics. In this work, we report on the first systematic experiments of this kind. Be proxy dust (Al, Cr, Cu) and W dust (as reference) was adhered in a controlled manner to well-defined regions of the same planar W substrates [12]. The samples were exposed in the Magnum-PSI linear plasma device under varying transient and steady state heat fluxes and different magnetic field topologies. The dust remobilization activities, macro-morphological changes and chemical modifications induced by the plasma have been documented. Implications regarding the survivability of adhered Be dust on hot W surfaces are discussed.

2. Experimental aspects

2.1. Sample composition and preparation

The outcome of the interaction of adhered dust with transient plasma fluxes strongly depends on the dust composition. Energy, momentum and particle exchange with the incident plasma as well as the substrate takes place, phase transitions and chemical changes may occur. Beryllium is characterized by a unique combination of thermomechanical and physicochemical properties. Consequently, it is impossible to identify a single appropriate proxy and a combination of surrogate materials has been selected [8, 15, 16]. Copper has similar adhesive properties and a close melting point, but a much higher thermal diffusivity and different mechanical, evaporation & chemical properties. Chromium has similar mechanical & adhesive properties and a close thermal diffusivity at high temperatures, but a higher melting point and different evaporation & chemical properties. Aluminium has similar chemical, evaporation & adhesive properties, but a lower melting point, a higher thermal diffusivity and different mechanical properties.

Four different dust populations were utilized in these experiments: **(i)** spheroidal Cu dust of a $\lesssim 5\,\mu$m nominal size range and a $\sim 3\,\mu$m mean diameter supplied by Goodfellow Cambridge Ltd, **(ii)** highly irregular flaky Cr dust of a $\lesssim 10\,\mu$m nominal size range and a $\sim 5\,\mu$m mean equivalent diameter supplied by Goodfellow Cambridge Ltd, **(iii)** spheroidal Al dust of a $\lesssim 10\,\mu$m nominal size range and a $\sim 4\,\mu$m mean diameter supplied by Schlenk Metallic Pigments GmbH, **(iv)** irregular W dust of a $\lesssim 1\,\mu$m nominal size range, but an actual $\lesssim 5\,\mu$m range with $\sim 2\,\mu$m mean equivalent diameter, supplied by Tungsteno S.n.c..

The W substrates were planar disks of 30 mm diameter, 1 mm thickness. All substrates were polished by sandpaper (P800 grade) in order to acquire similar surface roughness characteristics. The rms roughness was $R_q \sim 100\,$nm.

Dust was adhered to the substrates with gas dynamics methods in a controlled manner which mimics sticking as it occurs in tokamaks [12]. Pre-adhesion was localized with the aid of protective masks into circular deposition areas of 0.3 mm diameter. Each substrate contained 4 or 5 dust spots. The 4−spot samples featured four symmetric spots at a 2 mm distance from the geometric center, whereas the 5−spot samples featured an additional spot at the center.

2.2. Sample exposure and analysis

The samples were mounted on the actively cooled endplate of the Magnum-PSI linear plasma device which is capable of reproducing the conditions expected in the ITER divertor [17, 18]. In Magnum-PSI, transient plasma fluxes can also be superimposed on the steady state plasma background by means of a capacitor bank system connected in parallel with the DC power supply [18]. The multi-target holder was utilized for the perpendicular exposures (B-field parallel to surface normal, $\measuredangle B = 90°$) and the large target holder for the oblique exposures ($\measuredangle B = 20°$). The B-field was $B = 1.5\,$T (unless stated otherwise) and the steady state hydrogen plasma parameters at the column center varied in the $T_e = 2.5-3.2\,$eV, $n_e = (5.5-6.5)\times 10^{19}\,$m^{-3} ranges (as measured by Thomson scattering close to the endplate). The transient plasma heat loads had a triangular pulse shape, a $\sim 1\,$ms duration, a 2 or 4 Hz frequency and up to 50 consecutive pulses were attempted.

The surface temperature profile was monitored by an infra-red camera in combination with a multi-wavelength pyrometer [19]. The thermal response of the W substrates during exposures had the following characteristics: There was a steep temperature rise lasting up to $\sim 5\,$sec when the steady state was established. The thermal equilibrium temperature had a radial dependence owing to the Gaussian plasma profile and reached $T_s^{eq} \simeq 900-1200°$C at the column center. Afterwards, there was a gradual small T_s^{eq} decrease that is attributed to the corresponding B-field decrease over the discharge duration [17, 19]. As a result of the ELM-like pulse incidence, fast periodic temperature excursions were superimposed on T_s^{eq} with a typical $\Delta T_{ELM} \simeq 200-400°$C magnitude. We point out that these excursions should be much higher for dust and clusters due to the small imperfect thermal contact with the substrate. A detailed inverse modelling for the determination of the maximum parallel heat flux was not pursued. It was simply estimated from the analytic solution of the 1D heating equation for a triangular pulse (with constant material coefficients) [20]. The resulting $q_{\|} \simeq 110-230\,$MW/m^2 values should be treated as approximate, since both radial heat diffusion and the temperature dependence of the W thermophysical properties [21] have been neglected.

The dust spots of each sample were mapped before and after plasma exposure, by means of a scanning electron microscope (SEM). The elemental composition of selected substrate areas was also analyzed using energy dispersive X-ray spectroscopy (EDX).

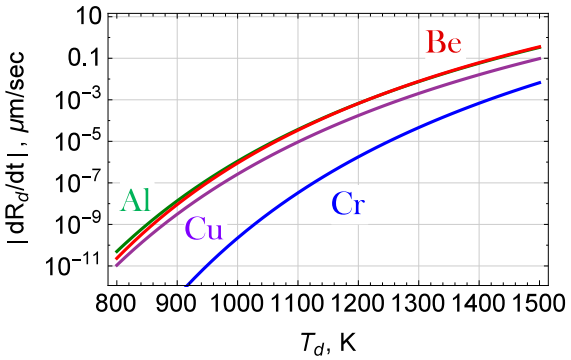

Figure 1: The size reduction rate owing to vaporization as a function of the temperature for Be, Al, Cu, Cr dust. The evaporation rate is described by the Hertz-Knudsen equation, which becomes $dR_d/dt = -\sqrt{m_{at}/(2\pi k_B T_d)}[p_{vap}(T_d)/\rho_m(T_d)]$ for spherical grains with k_B the Boltzmann constant, m_{at} the atomic mass, R_d the dust radius, T_d the surface temperature, ρ_m the mass density and p_{vap} the vapour pressure of the dust material. The $p_{vap}(T_d)$ dependence follows the semi-empirical expression $\log_{10}[p_{vap}(T_d)] = A - (B)/(C + T_d)$ with the material dependent coefficients adopted from Ref.[22]. Note that the Be, Al curves nearly overlap in the whole temperature range.

Table 1: Exposure statistics for μm size Be-proxy (Cu, Cr, Al) dust adhered to planar W substrates: $q_{\parallel}$ denotes the maximum parallel heat flux at the center of the plasma column (triangular pulse), T_s^{eq} the quasi-equilibrium substrate surface temperature, t_{exp} the exposure time measured from the establishment of thermal equilibrium and $\measuredangle B$ the angle between the magnetic field lines and the surface tangent. Summary of modifications induced by the incidence of Magnum-PSI transient and steady state hydrogen plasmas ($B = 1.5\,T$). There were some issues concerning the alignment of the plasma column center with the sample center, which were most prominent in the oblique exposures (compare the modifications induced in samples #7, 8). Hence, in spite of the cylindrical symmetry, the spots of the same sample were not always wetted by comparable particle and heat fluxes. Notice also that, during the most intense exposures, different regions of the W substrates underwent recrystallization.

Sample	$\measuredangle B$	ELMs	$q_{\parallel}$	T_s^{eq}	t_{exp}	Summary of SEM observations
#1	90°	1 ELM	110 MW/m^2	900°C	20 s	Cu: partial removal, molten traces Cr: no changes Al: total removal, parallelepiped structures
#2	90°	1 ELM	220 MW/m^2	1000°C	20 s	Cu: total removal, no traces Cr: wetting induced coagulation Al: total removal, parallelepiped structures
#3	90°	10 ELMs, 2 Hz	230 MW/m^2	900°C	20 s	Cu: low removal, wetting induced coagulation Cr: few wetting induced coagulation Al: total removal, parallelepiped structures
#4	90°	10 ELMs, 4 Hz	130 MW/m^2	900°C	20 s	Cu: total removal, no traces Cr: wetting induced coagulation Al: total removal, parallelepiped structures
#5	90°	50 ELMs, 2 Hz	230 MW/m^2	1200°C	35 s	Cu: total removal, no traces (recryst.) Cr: some removal, wetting induced coagulation Al: total removal, round structures (recryst.)
#6	90°	50 ELMs, 4 Hz	230 MW/m^2	1050°C	23 s	Cu: total removal, no traces Cr: mostly removal, wetting induced coagulation Al: total removal, intermediate structures
#7	20°	50 ELMs, 2 Hz	230 MW/m^2	-	30 s	Cu: total removal, no traces (recryst.) Cr: total removal, no traces (recryst.) Al: total removal, round structures (recryst.)
#8	20°	50 ELMs, 4 Hz	230 MW/m^2	-	20 s	Cu: no removal, wetting induced coagulation Cr: very few wetting induced coagulation Al: total removal, parallelepiped structures
#9	90°	steady state	-	1000°C	20 s	Cu: total removal, few molten traces Cr: no changes Al: total removal, intermediate structures

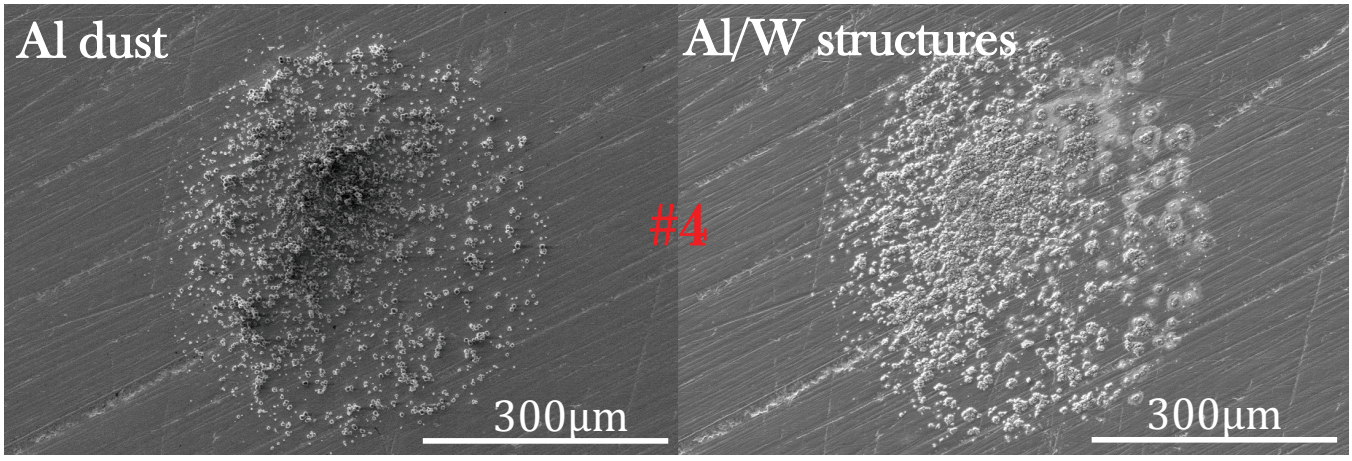

Figure 2: SEM images of the Al spot of sample #4 prior to and post perpendicular exposure to the transient Magnum-PSI hydrogen plasma. The adhered Al dust was fully removed from the W substrate leaving thin Al/W structures of "parallelepiped" morphology (see subsection 3.2 for details) beneath all the uncovered contact areas. A similar comparison of SEM images, prior to and post plasma exposure, can be found at the supplementary material for all the 36 spots.

3. Experimental results

3.1. Remobilization and macro-morphological changes

Overall, 9 exposures concerned the W samples which contained four dust spots (Cu, Cr, Al, W). The post-mortem observations have been summarized in Table 1. SEM images of all the 36 spots, prior to and post plasma exposure, can be found at the supplementary material. For Be and its proxies, the mass loss rate due to vaporization has been plotted in figure 1 as a function of the temperature.

Copper dust. The Cu melting point is 1085° C which is close to the equilibrium temperatures of the W substrate. The dust evaporated mass for the relevant temperatures and exposure times is not negligible, but complete vaporization could not have taken place even for the most intense plasma fluxes. Thus, unless remobilization occurred, adhered Cu dust must have remained molten during the longest part of most exposures due to the superimposed ELM-like heat pulses as well as the small contact area and imperfect thermal contact conductance. *After the weakest exposures* ($\#3, 8$), the remobilization rates were very low and wetting induced coagulation led to the transformation of clusters to nearly spherical large monomers. This implies that melting was achieved only during the ELM-like pulses and that the resolidification timescale was rather short compared to the pulse period. *After more intense exposures* ($\#1$), dust was partially removed by the plasma leaving thin melt layers with a $\sim 100\%$ Cu composition (as revealed by EDX) beneath some contact areas. These resolidified material traces strongly suggest that removal occurred while the dust grains were in the liquid state. It is very likely that the longer resolidification timescales and the elevated dust temperatures facilitated droplet ejection. *After the most intense exposures* ($\#2, 4, 5, 6, 7$), all dust was removed from the W substrate uncovering a pristine surface without material traces or surface irregularities. Most probably, the temperatures were high enough so that the thin melt layer, which survives droplet ejection, has fully vaporized. *After the steady state exposure* ($\#9$), dust was fully removed leaving thin melt layers beneath few of the contact areas whose composition is again $\sim 100\%$ Cu. It is evident that the underlying droplet release mechanism does not require for the plasma to be transient.

Chromium dust. The melting point of Cr is 1907° C which is higher than the equilibrium as well as transient temperatures acquired by the W substrate. Nevertheless, dust grains and especially clusters should have experienced short-lived melting during most exposures owing to the small contact area and imperfect thermal contact. Dust vaporization is always negligible for the relevant temperatures and exposure times, the radius decrease is estimated to be of the order of few 100 nm for the most intense plasma fluxes. *After the weakest exposures* ($\#1, 3, 8$), the remobilization rates were nearly zero and very few instances of wetting induced coagulation were discerned. ELM-induced melting events must have been infrequent and the resolidification times too short to lead to any macro-morphological changes. *After more intense exposures* ($\#2, 4$), the remobilization rates remained extremely low but the instances and extent of wetting induced coagulation greatly increased. The resolidification times remained rather short and thus Cr droplet ejection was still inhibited. *After the most intense exposures* ($\#5, 6, 7$), a varying amount of dust was removed from the sample: a small percentage in #5, the majority in #6, all in #7. All uncovered contact areas were chromium-free, as revealed by EDX. *After the steady state exposure* ($\#9$), neither remobilization nor macro-morphological changes took place.

Aluminium dust. Pure Al melts at 660° C which is lower than the equilibrium temperatures of the substrate. Assuming that dust remains adhered to the substrate during the whole exposure, the estimated dust radius decrease due to vaporization ranges from less than 10 nm to more than 5 μm. However, the results clearly imply that droplet release took place at the beginning of the discharges and thus vaporization could not have played a role even for the most intense exposures. *After all transient and steady state exposures* ($\#1-9$), dust was fully removed from the W substrate, see figure 2 for an example. The uncovered contact areas featured irregular thin complex structures which are composed of Al, W (as revealed by EDX) and whose morphology depends on the exposure conditions. These Al/W structures will be examined in subsection 3.2.

Tungsten dust. The W melting point is 3422° C which is much higher than the equilibrium and also the transient temperatures acquired by the W substrate. W dust vaporization is totally negligible, since W has the lowest vapor pressure at high temperatures. Heat transfer simulations have revealed that even large dust clusters should not melt under similar plasma conditions [23]. In addition, earlier Pilot-PSI experiments with adhered W dust strongly suggest that there should be nearly no remobilization of solid $\lesssim 5\,\mu$m W dust, see for instance Ref.[4]. *After all transient and steady state exposures* ($\#1-9$), neither remobilization nor any macro-morphological changes were observed, thus confirming the expectations. The purpose of these spots was to serve only as reference spots, verifying that sample transportation and mounting on the holder did not cause any differences in the original dust deposition profiles.

3.2. Composition and morphology of the Al/W structures

The thin Al melt residues, that remain on the W substrate after Al droplet release, should have promptly vaporized during all plasma exposures (as observed after the most intense exposures of Cu dust). Their post exposure presence suggests that significant interatomic diffusion has taken place and that even intermetallic compound formation has ensued. The latter possibility is supported by EDX, which revealed an Al/W stoichiometry ranging from 75/25 at.% to 10/90 at.%. Alloy formation is also expected from proposed phase diagrams of the binary system, where the intermetallic compounds $Al_{12}W$, Al_5W, Al_4W are formed by peritectic reactions [24, 25]. We emphasize though that

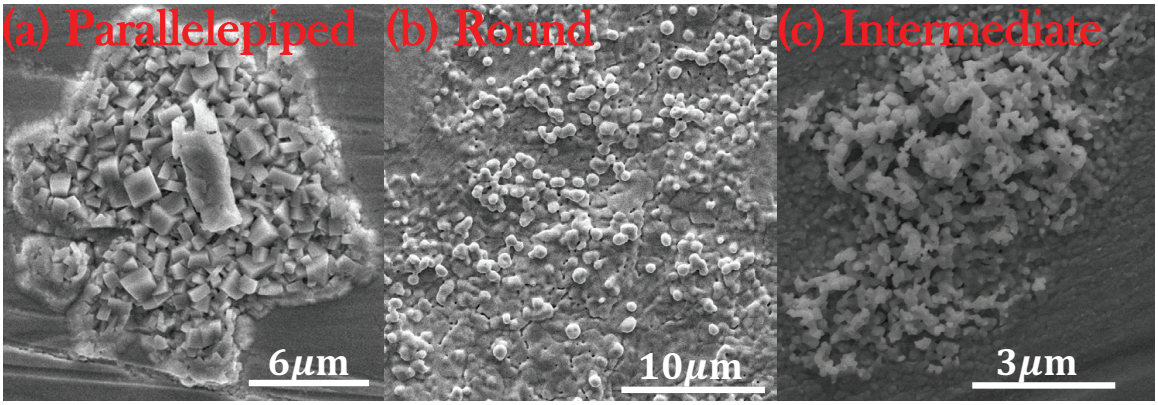

Figure 3: Zoom-in SEM images of three Al/W structures of different morphology which are formed after perpendicular exposure to the transient Magnum-PSI hydrogen plasma. (a) "Parallelepiped" structures in sample #2 ($T_s^{eq} \simeq 1000°$ C, $t_{exp} \simeq 20$ s). (b) "Round" structures in sample #5 ($T_s^{eq} \simeq 1200°$ C, $t_{exp} \simeq 35$ s). (c) "Intermediate" structures in sample #6 ($T_s^{eq} \simeq 1050°$ C, $t_{exp} \simeq 23$ s).

EDX is not a pure surface analysis technique, since it involves a $\sim 2\,\mu$m sample depth. Therefore, the EDX results could be characterized by a W-rich bias due to the underlying substrate, in the case that Al inter-diffusion is limited. For unambiguous results, a surface analysis technique such as X-ray photoelectron spectroscopy should be employed.

Three different morphologies of Al/W structures were discerned, as depicted in figure 3. Their realization does not depend on the transient heat flux, the number and frequency of ELM-like pulses or the B-field topology (see Table 1). There is only a strong dependence on the equilibrium substrate temperature (a weaker dependence on the plasma exposure time, which does not drastically vary among the present discharges, is also expected). For $T_s^{eq} \sim 900°$ C, the Al/W structures consist of parallelepiped pillars which can acquire a columnar shape and extend up to few μm. These structures can protrude up to a few μm above the substrate. For $T_s^{eq} \sim 1200°$ C, the Al/W structures consist of a sparse network of round-ended tendrils. The tendril length can even exceed $5\,\mu$m but the round edges are less than $1\,\mu$m. The structures hardly protrude above the substrate (1μm or less). For $T_s^{eq} \sim 1000°$ C, the Al/W structures have a rather intermediate morphology, consisting of dense network of thin pillars.

As suggested by the exposure of sample #9, Al droplet ejection and Al/W structure formation take place during the interaction with the steady state plasma and the effect of transient plasma incidence is rather limited. In order to strengthen this argument, three further steady state exposures were carried out that concerned W samples which contained five Al dust spots. Each exposure targeted a different equilibrium substrate temperature. The results are summarized in Table 2. Zoomed-in SEM images of the precursor W-adhered Al dust and the resulting Al/W structures are illustrated in figure 4. We point out that the Al content is strongly decreased for very high T_s^{eq} (competition between inter-diffusion and evaporation). Finally, sample #5 was re-exposed to steady state plasma and only minor further modifications were observed, see figure 5.

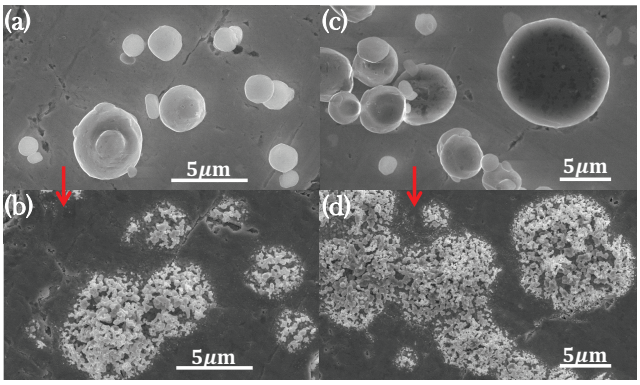

Figure 4: Zoom-in SEM images from two different Al spots of sample #10 prior to and post perpendicular exposure to the steady state Magnum-PSI hydrogen plasma. The correspondence is (a)→(b) and (c)→(d). The resulting Al/W structures have an intermediate morphology. All isolated dust (regardless of size) and clusters (regardless of the monomer constituents) led to the formation of Al/W structures. The Al/W footprint is much larger than the contact area but comparable with the size of the precursor dust indicating that the Al droplets did not fully spread on the substrate before their ejection.

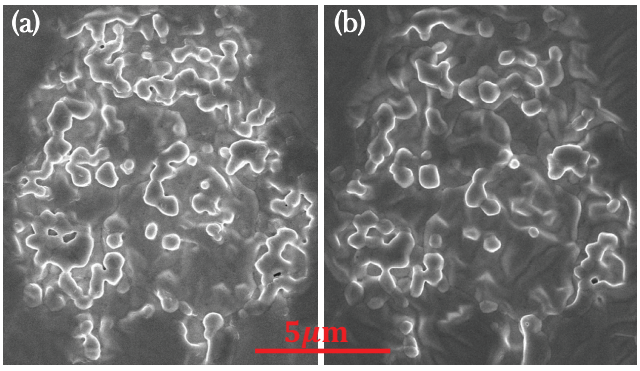

Figure 5: Zoom-in SEM images of the same Al/W structure of sample #5. (a) "Round" morphology resulting after perpendicular exposure to the transient Magnum-PSI hydrogen plasma ($N_{ELM} = 50$, $f_{ELM} = 2$ Hz, $q_{\|} \simeq 230$ MW/m^2, $T_s^{eq} \simeq 1200°$ C, $t_{exp} \simeq 35$ s). (b) Resilience of "round" morphology after perpendicular re-exposure to the steady state Magnum-PSI hydrogen plasma ($T_s^{eq} \simeq 1300°$ C, $t_{exp} \simeq 40$ s). Only minor further modifications can be detected that are confined in nanometer length-scales.

Table 2: Exposure statistics for μm size Al dust adhered to planar W substrates. Summary of modifications induced by the perpendicular incidence of steady state Magnum-PSI hydrogen plasmas. The B-field was 1.0 T for sample #10 and 1.3 T for samples #5, 11, 12. Notice that two W substrates not only underwent recrystallization but also cracked either during exposure or during dismounting.

Sample	T_s^{eq}	t_{exp}	SEM observations
#10	900°C	20 s	5 spots: total removal intermediate structures no recrystallization
#11	1500°C	40 s	5 spots: total removal round structures recrystallization, cracking
#12	1600°C	37 s	5 spots: total removal round structures recrystallization, cracking
#5	1300°C	40 s	1 spot: nearly unaltered re-exposed sample

4. Discussion

Qualitative picture. Courtesy of the large exposure statistics and the use of different dust materials, a qualitative picture has emerged concerning the physicochemical processes that take place during the interaction of beryllium proxy dust adhered on tungsten substrates with the transient and steady state plasma heat fluxes of Magnum-PSI. **(a)** In the case of low ($q_\parallel$, T_s^{eq}) values for which dust and even cluster melting is short-lived, nearly no remobilization instances and no macro-morphological changes occur. **(b)** In the case of modest ($q_\parallel$, T_s^{eq}) values for which cluster melting is more long-lived, wetting induced coagulation takes place but the remobilization activity remains rather low. **(c)** In the case of high ($q_\parallel$, T_s^{eq}) values for which the resolidification timescales become longer than the spreading timescales, partial droplet ejection takes place possibly leaving melt traces beneath the former contact areas. **(d)** In the case of higher ($q_\parallel$, T_s^{eq}) values for which the resolidification timescales are very long or for which dust melting becomes sustained, nearly 100% droplet release takes place and the melt residues either completely vaporize or react chemically with the W substrate. A quantification of the limiting ($q_\parallel$, T_s^{eq}) values that lead to transition between the four regimes (strongly depending on the dust material) is currently not possible. However, it is evident that in these exposures: Cu dust lies in regimes (b-c-d), Cr dust in all regimes, Al dust only in (d), W dust only in (a).

Extrapolation from proxy to beryllium dust. The phase diagrams of the respective binary systems should be first examined [24, 25]. Concerning **Cu-W**, the mutual solubilities are negligible and no intermetallic compounds form. In fact, as observed in these exposures, a pristine W substrate is uncovered after the complete removal of the Cu dust and melt traces. Concerning **Cr-W**, there is a miscibility gap $\lesssim 1650°$ C and no compounds are known. Again, the present experiments reveal that a pristine W substrate is uncovered after complete Cr dust removal. Concerning **Al-W**, three compounds ($Al_{12}W$, Al_5W, Al_4W) can form with the reaction initiating at $\sim 650°$ C. In fact, the exposures document the formation of Al/W structures of different morphology. Concerning **Be-W**, three compounds ($Be_{22}W$, $Be_{12}W$, Be_2W) can form with the reaction initiating at $\sim 750°$ C (note that room temperature initiation has also been reported [26]). Considering the above, as well as the nearly identical evaporation properties, Be dust will most probably exhibit a similar behavior with Al dust, *i.e.* complete removal and Be/W structure formation, albeit at higher ($q_\parallel$, T_s^{eq}) values given the 1287° C melting point.

Extrapolation from linear to fusion plasma devices. An overview of the large body of experimental evidence which are available for adhered W dust [4, 5, 7, 8, 11] suggests that similar phenomena should be observed in fusion devices with two basic differences: somewhat higher remobilization activities and the frequent occurrence of dust clustering and tangential displacements. In fact, wetting-induced coagulation was observed in ASDEX-Upgrade exposures of Cu, Cr dust [8] and Al/W structure formation was observed in DIII-D exposures of Al dust [11]. Extrapolations to ITER certainly involve some degree of speculation. However, the high heat flux areas of the water-cooled W divertor are currently predicted to acquire equilibrium temperatures close to the Be melting point under steady state loading [27, 28] and should exceed it under transient loading - even for successfully mitigated ELMs. As a consequence, it can be expected that regime (d) is realized, which implies that Be dust residing near the divertor strike point (transported after mitigated major disruptions and vertical displacement events) will be ejected in the form of droplets in the subsequent discharge. Hence, local Be dust accumulation is only possible inside the gaps and should be limited in light of relative surface area considerations. It should also be pointed out that Be dust will most likely engender mixed Be/W effects prior to its plasma removal.

Acknowledgments

This work has been carried out within the framework of the EUROfusion Consortium and has received funding from the Euratom research and training programme 2014-2018 under grant agreement No 633053. Work performed under WP PFC. The views and opinions expressed herein do not necessarily reflect those of the European Commission.

[1] J. P. Sharpe, D. A. Petti and H.-W. Bartels, *Fusion Eng. Des.* **63-64** (2002) 153
[2] J. Roth, E. Tsitrone, A. Loarte *et al.*, *J. Nucl. Mater.* **390-391** (2009) 1
[3] M. Shimada, R. A. Pitts, S. Ciattaglia *et al.*, *J. Nucl. Mater.* **438** (2013) S996
[4] S. Ratynskaia, P. Tolias, I. Bykov *et al.*, *Nucl. Fusion* **56** (2016) 066010
[5] S. Ratynskaia, P. Tolias, M. De Angeli *et al.*, *Nucl. Mater. Energy* **12** (2017) 569
[6] M. De Angeli, P. Tolias, S. Ratynskaia *et al.*, *Nucl. Mater. Energy* **12** (2017) 536

[7] V. Weinzettl, J. Matejicek, S. Ratynskaia *et al.*, *Fusion Eng. Des.* **124** (2017) 446
[8] S. Ratynskaia, P. Tolias, M. De Angeli *et al.*, *Nucl. Fusion* **58** (2018) accepted
[9] G. De Temmerman, R. A. Pitts, E. Veshchev and P. Shigin 2017 Issues with dust production for ITER *Eurofusion Science Meeting on Dust Physics (8 February 2017)*
[10] L. Vignitchouk, S. Ratynskaia, P. Tolias *et al.*, *Nucl. Fusion* **58** (2018) 076008
[11] I. Bykov, D. L. Rudakov, S. Ratynskaia *et al.*, *Nucl. Mater. Energy* **12** (2017) 379
[12] P. Tolias, S. Ratynskaia, M. De Angeli *et al.*, *Plasma Phys. Control. Fusion* **58** (2016) 025009
[13] S. Ratynskaia, L. Vignitchouk, P. Tolias *et al.*, *Nucl. Fusion* **53** (2013) 123002
[14] L. Vignitchouk, P. Tolias and S. Ratynskaia, *Plasma Phys. Control. Fusion* **56** (2014) 095005
[15] L. Marot, C. Linsmeier, B. Eren *et al.*, *Fusion Eng. Des.* **88** (2013) 1718
[16] P. Tolias, *Fusion Eng. Des.* **133** (2018) 110
[17] G. De Temmerman, M.A. van den Berg, J. Scholten *et al.*, *Fusion Eng. Des.* **88** (2013) 483
[18] T. W. Morgan, T. M. de Kruif, H. J. van der Meiden *et al.*, *Plasma Phys. Control. Fusion* **56** (2014) 095004
[19] T. W. Morgan, A. Vertkov, K. Bystrov *et al.*, *Nucl. Mater. Energy* **12** (2017) 210
[20] J. H. Yu, G. De Temmerman, R. P. Doerner *et al.*, *Nucl. Fusion* **55** (2015) 093027
[21] P. Tolias, *Nucl. Mater. Energy* **13** (2017) 42
[22] C. L. Yaws, *The Yaws Handbook of Vapor Pressure: Antoine Coefficients*, Elsevier, Oxford, 2015
[23] E. Thorén, MSc Thesis *Heating of Adhered Metallic Dust in Tokamaks*, Luleå University of Technology, Luleå, 2016
[24] B. Predel, Al-W (Aluminum-Tungsten), In: Madelung O. (eds) Ac-Au - Au-Zr. Landolt-Börnstein - Group IV Physical Chemistry vol 5a, Springer-Verlag, Berlin, 1991
[25] E. Lassner and W.-D. Schubert, 1999 Tungsten: Properties, Chemistry, Technology of the Element, Alloys, and Chemical Compounds, Kluwer, Dordrecht, 1999
[26] A. Wiltner and Ch. Linsmeier *New J. Phys.* **8** (2006) 181
[27] R. A. Pitts, S. Bardin, B. Bazylev *et al.*, *Nucl. Mater. Energy* **12** (2017) 60
[28] J. P. Gunn, S. Carpentier-Chouchana, F. Escourbiac *et al.*, *Nucl. Fusion* **57** (2017) 046025